The Solubility of Uranophane under Oxidizing Conditions in $CaCl_2$ and SiO_2(aq) Test Solutions

James D. Prikryl[1,*] and William M. Murphy[2]

[1]Center for Nuclear Waste Regulatory Analyses, Southwest Research Institute, 6220 Culebra Road, San Antonio, Texas 78238-5166

[2]Department of Geosciences, California State University, Chico, California 95929-0205

Uranophane / Solubility / Synthesis / Oxidizing conditions / Yucca Mountain

Summary. Uranophane [$Ca(UO_2)_2Si_2O_7 \cdot 6H_2O$] is a corrosion product of long-term leaching of spent fuel under oxidizing conditions and is a weathering product of uraninite in uranium ore deposits hosted by siliceous volcanic rocks. The solubility of uranophane may, therefore, play an important role in radionuclide release at the proposed nuclear waste repository at Yucca Mountain, Nevada. In this study, the solubility of uranophane in Ca- and Si-rich test solutions was investigated. Batch solubility experiments were designed to approach uranophane equilibrium in both undersaturated and supersaturated solutions that had initial U concentrations of 10^{-5} to 10^{-7} mol $\cdot$ L^{-1} in matrices of 10^{-2} mol $\cdot$ L^{-1} $CaCl_2$ and 10^{-3} mol $\cdot$ L^{-1} SiO_2(aq). Experimental solutions were reacted with synthetic uranophane (confirmed by XRD and chemical analyses) and analyzed at 1-week intervals over 7 weeks. A drop in solution pH and strong Ca precipitation in solutions with higher initial U concentrations characterized initial reaction of uranophane with experimental solutions. After the initial effect, reaction paths were dominated by uranophane dissolution coupled to uranyl mineral precipitation. Calculated reaction quotients (log Qs) for uranophane dissolution were related to solution pH and ranged from 10.89 to 14.62. Based on higher solution pH, test solutions with lower initial U contents ended closer to the solubility limit of uranophane. However, continued uranophane dissolution indicated that test solutions at the ends of the experiments were undersaturated with respect to uranophane.

Introduction

Under oxidizing aqueous conditions, uraninite (UO_2) and spent nuclear fuel (generally greater than 95% UO_2) are thermodynamically unstable and will undergo dissolution leading to the formation of secondary uranyl phases. Crystallographic theory and experimental data indicate that spent fuel waste species (e.g., Np) may be incorporated in the structures of relatively stable secondary uranyl phases [1, 2]. The solubilities of secondary uranyl minerals may, therefore, play an important role in constraining the source term for radionuclide release from high-level nuclear waste (HLW) repositories. For example, in recent performance assessments conducted by the Center for Nuclear Waste Regulatory Analyses for the proposed

* Author for correspondence (E-mail: jprikryl@swri.edu)

HLW geologic repository at Yucca Mountain (YM), Nevada, a source term model is included based on the assumption that radionuclides from the spent fuel matrix become incorporated in the oxidized secondary uranium mineral schoepite. Radionuclide releases then occur in proportion to the solubility-limited dissolution of schoepite [3-5].

Studies of uranium (U) deposits that are natural analogs to the proposed high-level nuclear waste repository at YM (e.g., deposits in the Peña Blanca Uranium District of Chihuahua, Mexico) indicate that the calcium uranyl silicate, uranophane [$Ca(UO_2)_2Si_2O_7 \cdot 6H_2O$] is the end product of U mineralization hosted by siliceous volcanic rocks [6]. Similarly, long-term leaching studies of synthetic UO_2 and spent UO_2 fuel designed to mimic conditions in a YM repository indicate that uranophane is a probable end product of the alteration of spent nuclear fuel [7, 8]. Natural uranophane has been noted to incorporate Th [9]. Therefore, uranophane that is secondary after spent fuel could incorporate part of the nuclear waste inventory and control its release from the engineered barrier system. However, the lack of, and often conflicting, thermodynamic data for uranyl minerals hamper predictive modeling of uranyl mineral formation and dissolution.

In this study, the solubility of uranophane under oxidizing conditions was studied by reacting uranophane with Ca- and Si-rich solutions calculated to bracket uranophane solubility. Reasonable interpretation of solubility data requires experimental samples to be relatively pure, single-phase minerals of known composition and structure. Although natural uranophane samples are available, they are typically of insufficient quantity or purity for use in solubility experiments [10]. Moreover, crystal defects in natural samples, which may be present due to radiation damage, could adversely affect the results of the experiments. Thus, experiments were performed using synthesized uranophane, whose synthesis and chemistry are described in this paper.

Experimental

Uranophane synthesis and characterization

Uranophane was synthesized based on the method of Cesbron et al. [11] using reagent grade uranyl acetate [$UO_2(CH_3COO)_2 \cdot 2H_2O$], sodium metasilicate [$Na_2SiO_3 \cdot 9H_2O$], and calcium acetate [$Ca(CH_3COO)_2 \cdot H_2O$]. About 105 g of the reagents in the stoichiometric ratio Ca:U:Si = 1:2:2 were placed in a teflon-lined

stainless steel reaction vessel. Then about 1,350 g of deionized, degassed water (with pH lowered to ~1.0 by addition of HCl) were added to the vessel. The vessel was sealed and evacuated to remove air. The temperature was raised to 150 °C and the reaction was allowed to proceed for 10 days. After cooling, the supernatant liquid was decanted. The solid product was washed several times with deionized water, dried in an oven at about 60 °C, and stored in a dessicator at room temperature (20.5 ± 2.0 °C).

An X-ray powder diffraction (XRD) pattern of the synthetic uranophane is shown in Fig. 1, together with a reference pattern for natural uranophane taken from the International Centre for Diffraction Data (ICDD) database [12]. Correspondence between the sample and reference patterns is good. Two small peaks (at 26.9° and 28.2° 2θ) appear in the pattern for the synthetic sample and are absent in the reference pattern. However, these peaks are reported in a reference pattern for natural uranophane (Powder Diffraction File Number 8-442) from the ICDD Minerals Data Book [13] and appear in uranophane synthesized by Nyugen et al. [14]. The magnitude and sharpness of the peaks in the XRD pattern indicate that the synthesized material is well crystallized. Fig. 1 also includes a scanning electron photomicrograph showing the fine-grained character and acicular morphology of the synthesized uranophane.

Chemical analyses of synthetic uranophane were performed using a whole rock procedure that entails a complete dissolution of the sample in 0.1 M HCl followed by inductively coupled plasma mass spectrometry (ICP-MS). Using measured analytical contents, stoichiometric coefficients for Ca:U:Si in the synthesized uranophane were calculated to be 0.99(±0.01):2.01(±0.01):2.01(±0.01). The Ca, U, and Si stoichiometry of the synthesized uranophane corresponds closely to the values expected for ideal uranophane (1:2:2, respectively). The Na content of the uranophane was 0.11(±0.02) ppm and indicates that only minor Na is incorporated in the uranophane.

Solubility experiments

Solubility experiments were designed to approach uranophane equilibrium in both undersaturated and supersaturated solutions. Estimation of the standard state Gibbs free energy of formation of uranophane by a theoretical method of prediction [15], together with data for aqueous species from the EQ3/6 Data0.com.R2 database [16], was used to estimate the equilibrium solution chemistry for uranophane. The Data0.com.R2 database adopts properties of aqueous uranium species from Grenthe et al. [17] and, together

with the EQ3NR geochemical code (version 7) [16], was used in all aqueous speciation calculations in this study.

Based on the above estimate, EQ3NR was used to determine starting solution compositions for the solubility experiments. Experimental solutions had initial U concentrations of 10^{-5} to 10^{-7} mol · L^{-1} in matrices of 10^{-2} mol · L^{-1} $CaCl_2$ and 10^{-3} mol · L^{-1} SiO_2(aq). Before addition of uranophane, the pH of experimental solutions were adjusted to ~6.0 by addition of $CaCO_3$ and allowed to equilibrate with atmospheric CO_2(g) for 2 weeks. The U concentration and pH of the experimental solutions before reaction with uranophane are shown in Table 1. The solubility experiments were carried out by reacting measured volumes of these solutions (100 ml) with measured amounts of synthetic uranophane (0.5 g) in 250 ml polycarbonate bottles. Experiments were conducted at room temperature (20.5 ± 2.0 °C) under atmospheric PCO_2 conditions. Solutions were continuously mixed during the experiments using a gyratory shaker.

Aliquots (5 ml) of the experimental solutions were taken at 1 week intervals over 7 weeks. The aliquots were passed through 0.45 μm syringe filters during the sampling procedure. Experimental solution weights were measured before and after each sampling to track loss of solution due to sampling and evaporation. The pH of sample aliquots were measured immediately upon sampling using a glass combination pH electrode (Orion) previously calibrated using commercial buffer solutions (Fisher Scientific). After pH measurement, sample aliquots were acidified to pH < 2.0 by addition of concentrated HNO_3. Concentrations of major cations in starting solutions and sample aliquots were determined by ICP; U concentrations were measured by ICP-MS.

Results

Experimental Data

Separate uranophane solubility experiments are defined by their starting U concentrations and are referred to by the test labels listed in Table 1. For example, test A refers to experimental solutions from the experiment with a starting U concentration of 10^{-5} mol · L^{-1}. The pH and concentrations of Ca, Si, and U measured in the test solutions as a function of reaction time are plotted in Fig. 2. Initial pH and initial Ca, Si, and U concentrations in the test solutions before addition of uranophane are plotted at time 0.

Plots of solution pH show a reduction in pH upon addition of uranophane to the experimental solutions (Fig. 2). At the 1 week sampling interval, the pH of solutions ranged from 5.48 to 5.67. After this initial reduction, the pH of experimental solutions in tests A and B remained relatively constant over the duration of the experiments. On the other hand, the pH of solutions in tests C, D, and E increased steadily until reaching stable pH of 6.68 to 6.80 at 6 to 7 weeks.

An initial reduction in the U and Ca contents of experimental solutions in tests A, B, and C is observed at the 1 week sampling interval (Fig. 2). A reduction in Ca content and increase in U content in test D is observed at the 1 week sampling interval. Test E shows an increase in U and Ca at the 1 week sampling interval. After 1 week, Ca concentrations increased linearly in all the solutions over the duration of the tests. Similarly, Si concentrations steadily increased linearly in all the solutions over the duration of the experiments. It should be noted that experimental solutions were in contact with air so increases in the concentrations of Ca and Si are due in part to evaporation.

U concentrations in experimental solutions fluctuated over the 7 week duration of the experiments. Analytical uncertainties in the measured U concentrations are 10%; therefore, fluctuations in U concentrations cannot be completely accounted for by analytical errors. Due to the very fine-grained character of the synthesized uranophane (see Fig. 1), the fluctuating U contents could have resulted from contamination by uranophane colloids (submicron-sized grains), which were not retained on the 0.45 μm membranes used to filter experimental solutions.

Mass Transfer Calculations

Thermodynamic and kinetic interpretation of the uranophane solubility data require knowledge of mass transfer (i.e., moles of Ca, Si, and U released or precipitated) as a function of time and solution chemistry. The cumulative release in a dissolution or precipitation experiment is given by

$$n_{I,R}(t_s) = m_I(t_s)W(t_s) + n_{I,E}(t_s) - m_I(t_0)W(t_0) \quad (1)$$

where $n_{I,R}(t_s)$ is the net number of moles of a component I (e.g., Ca, Si, or U) released to solution at the time of sampling (t_s) which is negative for net precipitation, $m_I(t_s)$ is the molality of I in the solution at time t_s, $m_I(t_0)$ is the molality of I in solution at the start of the experiment (t_0), $W(t_s)$ is the mass of solvent prior

to sampling at time t_s, $W(t_0)$ is the mass of solvent at time t_0, and $n_{I,E}(t_s)$ is the number of moles of I extracted in all solution samples removed at all times t_p prior to time t_s, which is given by

$$n_{I,E}(t_s) = \Sigma\, m_I(t_p) W_E(t_p) \tag{2}$$

where $m_I(t_p)$ is the molality of I in solution taken at time t_p and $W_E(t_p)$ is the mass of solution extracted in the sample taken at time t_p. Measurements of experimental solution masses before and after sampling provide values of W and W_E, which allow effects of variations in solution mass due to sampling and evaporation to be explicitly accounted for in the cumulative mass transfer calculations.

Results of the mass transfer calculations for Ca, Si, and U in each of the uranophane solubility tests are illustrated in Fig. 3. The data indicate net precipitation of Ca, Si, and U at the 1 week sampling interval in tests A, B, and C. Precipitation of Ca and net release of Si and U are observed in test D at the 1 week sampling interval. Test E showed net releases of Ca, Si, and U at the 1 week sampling interval.

After the initial sampling interval (1 week), all the tests showed gains in the number of moles of Ca and Si released up to the 5 week sampling interval (Fig. 3). After the 5 or 6 week sampling interval, a decrease in the number of moles of Ca released was observed whereas the number of moles of Si released tended to remain relatively constant. Like U concentrations in the experimental solutions, moles of U released in all the tests fluctuated but remained relatively constant over the 7 week duration of the experiments.

Thermodynamic Calculations

The dissolution reaction for uranophane can be written as

$$Ca(UO_2)_2Si_2O_7 \cdot 6H_2O + 6H^+ \Leftrightarrow Ca^{2+} + 2UO_2^{2+} + 2SiO_2(aq) + 9H_2O. \tag{3}$$

The corresponding reaction quotient for uranophane dissolution is defined by

$$Q = [Ca^{2+}]\,[UO_2^{2+}]^2\,[SiO_2(aq)]^2\,[H^+]^{-6} \tag{4}$$

where the square brackets represent thermodynamic activities corresponding to a standard state of a one molal solution referenced to infinite dilution. Using the pH and concentrations of Ca, Si, and U measured in the experimental solutions and assuming equilibrium with atmospheric PCO_2, activities of the aqueous

species in equation 4 were determined using EQ3NR. Reaction quotients for the experiments were then calculated using equation 4.

Solution pH, logarithms of the activities of Ca^{2+}, $SiO_2(aq)$ and UO_2^{2+}, and calculated logarithms of reaction quotients for uranophane (log Qs) obtained from solution chemistries at the 5 to 7 week sampling intervals are listed in Table 2. The data indicate that activities of Ca^{2+} and $SiO_2(aq)$ were relatively constant at the ends of the experiments. However, the activities of UO_2^{2+} varied widely; log activities of UO_2^{2+} ranged from –9.49 to –6.51. Based on output from EQ3NR, UO_2^{2+} activities were lower in tests C, D, and E due to the formation of uranyl hydroxide and uranyl-hydroxy-carbonate species [e.g., $UO_2(OH)_3^-$ and $(UO_2)_2CO_3(OH)_3^-$] in solutions at higher pH. Reaction quotients in Table 2 cluster into two groups, which are related to solution pH and to a lesser extent UO_2^{2+} activity variations. Test A and B solutions have calculated log Qs ranging from 10.89 to 11.83 and pH from 5.44 to 5.65. The calculated log Qs for test C, D, and E solutions ranged from 13.76 to 14.62 with pH from 6.57 to 6.80.

Interpretation

Experiments were designed to bracket the uranophane solubility limit and to approach equilibrium from undersaturated and supersaturated conditions. Although chemical conditions were selected to limit possible complications, mass transfer and thermodynamic analyses indicate that experimental results were considerably more complicated. Distinct types of reaction paths, which will be called A-type and E-type, were followed by test solutions with higher and lower initial U concentrations, respectively. The A-type experiments (represented by tests A and B) were characterized by initial precipitation of Ca, Si, and U, net precipitation of Ca and U throughout the course of the experiments, and relatively constant low pH after the first week of reaction. The E-type experiments (represented by tests D and E) were characterized by net release of Ca and U and an increase in pH after the first week of reaction. Test C solutions had characteristics transitional between the A- and E-type experiments (e.g., initial precipitation of Ca, Si, and U and net precipitation of Ca over the course of the experiment, but an increase in pH after the first week of reaction and net U release at the end of the experiment).

On addition of uranophane to the test solutions the pH initially dropped in all experiments (Fig. 2a). Initial pH reduction was largely independent of the initial dissolved uranyl concentrations, suggesting a surface phenomenon such as hydroxide sorption on a positively charged uranophane surface or Ca^{2+}

exchange with surface H^+. Uranophane was synthesized under acidic conditions, which may have resulted in a positive surface charge. In A-type experiments, pH did not recover from its initial drop from about 6 to 5.5. In the E-type experiments, after its initial drop, the pH rose to values in excess of 6.5.

Despite two orders of magnitude difference in initial U concentrations, measured U concentrations were remarkably similar; initial differences were largely eliminated after the first week of reaction (Fig. 2d). Uranium analyses included a number of apparently erratic data. In the A-type experiments U data were particularly scattered perhaps due to the influence of U colloids in solution with initially high U concentrations. In the E-type experiments there were a few apparently anomalously high measurements interrupting generally smooth trends in the data (e.g., at 2 weeks in test D and 3 weeks in test E).

Although total U concentrations tended toward values in a limited range, uranyl (UO_2^{2+}) activities between the A- and E-type experiments, as determined using EQ3NR, varied widely due to differences in pH and aqueous uranyl hydroxide and carbonate speciation relations. Uranyl activities were lower in the E-type experiments due to the formation of uranyl-hydroxide and uranyl-hydroxy-carbonate species [e.g., $UO_2(OH)_3^-$ and $(UO_2)_2CO_3(OH)_3^-$] in solutions at higher pH.

Initial precipitation of Ca in the A-type experiments was accompanied by precipitation of Si and U (Fig. 3). However, when compared to U and Si, the reduction in dissolved Ca is too great to be accounted for by uranophane precipitation. For example, U precipitation was less than Ca by factors of 40 and 200 in tests A and B, respectively. On the other hand, the initial Si precipitation was comparable to that of U suggesting precipitation of a uranyl silicate.

After a small amount of Si precipitation during the first week of reaction in the A-type experiments, there was net release of Si through week 6 in all the test solutions (Fig. 3b). The only possible source for Si is uranophane, so solutions generally remained undersaturated with respect to uranophane. In contrast, after initial U precipitation in the A-type experiments, net U release remained approximately constant in the test solutions over the course of the experiments (Fig. 3c). The behavior of Si and U in the test solutions suggests that uranophane dissolution was balanced by uranyl mineral precipitation. This process conserved U such that net U release and U concentrations in solution were steady.

A plot of net moles of Ca released versus net moles of Si released from each test is presented in Fig. 4. The data in Fig. 4 indicate that release of Ca and Si was not stoichiometric during the early stages

of the tests (1-4 weeks). The dashed lines in Fig. 4 have slopes of 0.5 and 2.0 and are included for illustrative purposes. Slopes of lines drawn through data points for weeks 1 to 3 in each test would have slopes of about 1.0 or greater, which do not correspond to the mole ratio of Ca to Si in uranophane (ideally 0.5).

Excess Ca in relation to Si released in the test solutions strongly suggests precipitation of a secondary Si-bearing phase or phases. Calculation of mineral saturation states in the test solutions using EQ3NR indicated supersaturation with the uranyl silicate soddyite [$(UO_2)_2SiO_4 \cdot 2H_2O$] and saturation with amorphous silica. However, XRD analyses of solids recovered from each test container at the end of the experiments were unable to detect the presence of any secondary mineral formation. The mineral saturation state calculations also indicated that test solutions were strongly undersaturated with respect to calcite and other U-free Ca minerals so the fate of excess Ca precipitation is unexplained.

The log activities of $UO_2^{2+}/(H^+)^2$ versus SiO_2 (aq) in test solutions for the last 4 sampling intervals (i.e., samples taken at 4 to 7 weeks) with respect to the solubility limits of soddyite and schoepite are plotted in Fig. 5a. The solubility limit of soddyite is based on data from Chen et al. [15] and the schoepite solubility limit is based on data from Grenthe et al. for $UO_2 \cdot 2H_2O$(s) [17]. This diagram shows that solution activities tended toward a limit corresponding to equilibrium with soddyite. The log activity of $UO_2^{2+}/(H^+)^2$ versus SiO_2 (aq) calculated using EQ3NR from experimental data from a soddyite dissolution experiment reported by Nguyen et al. [14] is also included in Fig. 5a. This datum is in general agreement with solution chemistries from the present study and soddyite solubility.

After initial precipitation of Ca and drop in pH, a reasonable interpretation is that reaction paths in both the A- and E-type experiments were dominated by uranophane dissolution coupled to uranyl mineral precipitation. Higher initial U concentrations and strong initial Ca precipitation in the A-type experiments appear to have inhibited uranophane dissolution. Due primarily to the increase in pH, the log Qs for uranophane dissolution were greater in the E-type experiments (13.76 to 14.62) than for the A-type experiments (10.89 to 11.83). Evidence for continued uranophane dissolution at the end of all the experiments indicates that all solutions are undersaturated with uranophane and, thus, the log Q values are all smaller than the equilibrium constant for uranophane dissolution. However, solutions in the E-type experiments came closer to uranophane solubility because of higher pH.

A logarithmic activity diagram of $UO_2^{2+}/(H^+)^2$ versus SiO_2 (aq) versus $Ca^{2+}/(H^+)^2$ illustrating the position of E-type solution chemistries for the last 4 sampling intervals with respect to the solubility limit of uranophane, as derived from theoretical prediction [15], are plotted in Fig. 6. The uranophane solubility limit shown was calculated using an equilibrium constant (log K) for uranophane of 12.30, which was derived from reaction 3 and an estimated standard state free energy of formation of uranophane (–6189.2 $kJ \cdot mol^{-1}$) reported by Chen et al. [15]. Fig. 6 shows that solution chemistries in the E-type experiments lie above the predicted solubility limit of uranophane. However, if test solutions in the present study are indeed undersaturated with respect to uranophane, then the log K for uranophane derived with data from Chen et al. [15] is too low.

Efforts to measure uranophane solubility have proven to be difficult in this study and in previous studies. Nguyen et al. [14] conducted a dissolution experiment using synthesized uranophane and reported a log K of 9.4 ± 0.5 for the reaction shown in reaction 3. This value was derived from a single experimental solution from an experiment conducted at low pH (3.50 ± 0.05) under an Ar atmosphere. Murphy and Pabalan [10] concluded that the uranophane solubility data reported by Nguyen et al. [14] are unreliable due to the non-nominal stoichiometric solid phase composition of the synthesized uranophane and incongruent elemental release in the dissolution experiments. Measured concentrations of U and Si in the synthesized uranophane agreed well with the nominal stoichiometric values for uranophane, but Ca was lower than the stoichiometric value. Like the present study, reported concentrations of Si, U, and Ca in the experimental solutions suggest incongruent elemental release, which probably resulted from secondary phase precipitation.

The log K values for uranophane from dissolution experiments conducted by Perez et al. [18] range from 10.75 to 12.94, with an average of 11.7 ± 0.6, for the reaction

$$Ca(UO_2)_2Si_2O_7 \cdot 6H_2O + 6HCO_3^- \Leftrightarrow Ca^{2+} + 2UO_2(CO_3)_3^{4-} + 2H_4SiO_4 + 5H_2O. \quad (5)$$

This study was carried out in bicarbonate solutions in contact with air, which had equilibrium pH ranging from 8.65 to 9.37. The uranophane used in these experiments was synthesized following the procedure of Nguyen et al. [14] and chemical analysis again showed a deficiency in Ca while Si and U contents corresponded well to the stoichiometry of uranophane. The reported stoichiometry of the synthesized

uranophane was Ca:Si:U = 0.8:2:2; however, ideal uranophane stoichiometry was assumed in the thermodynamic analysis, which introduces substantial error in the determination of the equilibrium constant. Although carbonate speciation was purported to have been calculated by Perez et al. [18], the calculated activities of aqueous uranyl species were apparently not used in the equilibrium constant determinations. Instead, it is asserted that for certain experiments the tris-carbonato-uranyl species $[UO_2(CO_3)_3^{4-}]$ is dominant, and all dissolved U was attributed to this species. Equilibrium constants were calculated assuming congruent dissolution; but, in general, only dissolved U was analyzed in the experimental solutions. Reference is made to a few Ca and Si analyses, and it is stated that these data showed the assumption of congruent dissolution to be correct, but no data are presented.

No satisfactory reversed low temperature uranophane solubility measurements appear to exist in the literature. Difficulty in determination of a reversed solubility for uranophane in this study contrasts conceptually with the widespread occurrence of uranophane in oxidizing low temperature U deposits [6, 19]. Our understanding of uranyl phase formation in these deposits is complicated by a lack of data on the chemistry and temperature of fluids that altered the primary U mineralization. Perhaps reactions leading to the precipitation of uranyl phases require elevated temperatures to proceed. Although aqueous U speciation as a function of pH and CO_2 is, in general, well understood [17], the role of uranyl hydroxide and carbonate species in solid phase formation at near-neutral to alkaline pH is poorly understood.

At the Nopal I deposit in the Peña Blanca Mining District of Chihuahua, Mexico, oxidative alteration of uraninite has resulted in a secondary uranyl mineral assemblage dominated by uranophane [6]. Petrographic and optical examination of specimens from Nopal I indicate that uranophane precipitation may require a uranyl or uranyl-silicate substrate to nucleate. For example, in specimens containing both dehydrated schoepite and uranophane, uranophane is generally observed to have formed after dehydrated schoepite. Preservation of textural features present in dehydrated schoepite, such as microcracks, in uranophane at Nopal I suggests a replacement process [6]. It is notable that ^{237}Np, a long-lived radionuclide that may affect the long-term safety of the proposed YM HLW geologic repository, has been identified in dehydrated schoepite formed in spent UO_2 fuel alteration experiments [2, 8]. From the standpoint of regulatory concern, the incorporation of Np into uranophane during replacement of dehydrated schoepite may provide a long-term mechanism for Np retention.

Conclusions

Uranophane solubility was studied by reacting synthesized uranophane with solutions designed to be both undersaturated and supersaturated with uranophane. Chemical analyses of the synthesized uranophane indicates that its stoichiometry corresponds to that expected for ideal uranophane (i.e., Ca:Si:U = 1:2:2). Experimental solution chemistries had initial U concentrations of 10^{-5} to 10^{-7} mol · L^{-1} in matrices of 10^{-2} mol · L^{-1} $CaCl_2$ and 10^{-3} mol · L^{-1} SiO_2(aq). Mass transfer and thermodynamic analyses indicated that distinct types of reaction paths (A-type and E-type) were followed by systems with higher and lower initial U concentrations. A-type experiments having initial U contents of 10^{-5} and 3.2 x 10^{-6} mol · L^{-1} were characterized by initial precipitation of Ca, Si, and U, net precipitation of Ca, and relatively constant pH after the first week of reaction. E-type experiments having initial U contents of 10^{-7} and 3.2 x 10^{-7} mol · L^{-1} were characterized by net release of Ca, Si, and U and an increase in pH after the first week of reaction.

Subsequent to an initial pH drop and strong Ca precipitation in the A-type experiments, reaction paths were dominated by uranophane dissolution coupled to uranyl mineral formation. Dissolution was greater in the E-type experiments characterized by increase in pH and greater release of Ca and Si. Higher initial U and strong initial Ca precipitation inhibited uranophane dissolution in the A-type experiments. Uranyl mineral precipitation was balanced by uranophane dissolution, which generally conserved U such that net U release and U concentrations in solution were steady. Excess Ca in solution with respect to Si suggests precipitation of a uranyl silicate, such as soddyite.

Log Q values for uranophane dissolution were greater for the E-type experiments (13.76 to 14.62) than for the A-type experiments (10.89 to 11.83) primarily due to higher pH at the end of the E-type experiments. Based on mass transfer analyses, uranophane continued to dissolve at the ends of all the experiments indicating that all values of log Q are smaller than the equilibrium constant for uranophane dissolution. However, the E-type experiments came closer to uranophane solubility because of increased pH. Difficulty in achieving uranophane equilibrium in this study contrasts with the widespread occurrence of uranophane in oxidizing, low temperature U deposits and highlights the challenges of determining the thermodynamic properties of uranyl minerals in similar systems.

Acknowledgements

Reviews by David R. Turner and Budhi Sagar are gratefully acknowledged. This work was funded by the Nuclear Regulatory Commission (NRC) under Contract No. NRC-02-97-009. The report is an independent product of the Center for Nuclear Waste Regulatory Analyses (CNWRA) and does not necessarily reflect the views or regulatory position of the NRC. Original data contained in this study meet quality assurance (QA) requirements described in the CNWRA QA manual.

References

1. Burns, P. C., Ewing, R. C., Miller, M. L.: Incorporation Mechanisms of Actinide Elements into the Structures of U^{6+} Phases Formed during the Oxidation of Spent Nuclear Fuel. Journal of Nuclear Materials 245, 1-9 (1997).
2. Buck, E. C., Finch, R. J., Finn, P. A., Bates, J. K.: Retention of Neptunium in Uranyl Alteration Phases Formed during Spent Fuel Corrosion. In: Scientific Basis for Nuclear Waste Management XXI (I. G. McKinley and C. McCombie, eds.). Materials Research Society Symposium Proceedings 506, 87-94, Warrendale, PA (1998).
3. Nuclear Regulatory Commission: NRC Sensitivity and Uncertainty Analyses for a Proposed HLW Repository at Yucca Mountain, Nevada, Using TPA 3.1 Volume 1: Conceptual Models and Data. NUREG-1668, v. 1 (1999).
4. Nuclear Regulatory Commission: NRC Sensitivity and Uncertainty Analyses for a Proposed HLW Repository at Yucca Mountain, Nevada, Using TPA 3.1 Results and Conclusions. NUREG-1668, v. 2 (1999).
5. Murphy, W. M., Codell, R. B.: Alternate Source Term Models for Yucca Mountain Performance Assessment Based on Natural Analog Data and Secondary Mineral Solubility. In: Scientific Basis for Nuclear Waste Management XXII (D. J. Wronkiewicz and J. Lee, eds.). Materials Research Society Symposium Proceedings 556, 551-558, Warrendale, PA (1999).
6. Pearcy, E. C., Prikryl, J. D., Murphy, W. M., Leslie, B. W.: Alteration of Uraninite from the Nopal I Deposit, Peña Blanca District, Chihuahua, Mexico, Compared to Degradation of Spent Nuclear Fuel in the Proposed U.S. High-Level Nuclear Waste Repository at Yucca Mountain, Nevada. Applied Geochemistry 9, 713-732 (1994).
7. Wronkiewicz, D. J., Bates, J. K., Gerding, T. J., Veleckis, E., Tani, B. S.: Uranium Release and Secondary Phase Formation During Unsaturated Testing of UO_2 at 90°C. Journal of Nuclear Materials 190, 107-127 (1992).
8. Finch, R. J., Buck, E. C., Finn, P. A., Bates, J. K.: Oxidative Corrosion of Spent UO_2 Fuel in Vapor and Dripping Groundwater at 90 °C. In: Scientific Basis for Nuclear Waste Management XXII (D. J. Wronkiewicz and J. Lee, eds.). Materials Research Society Symposium Proceedings 556, 431-438, Warrendale, PA (1999).
9. Frondel, C.: Systematic Mineralogy of Uranium and Thorium. Geological Survey Bulletin 1064, U. S. Geological Survey, Washington, D. C. (1958).
10. Murphy, W. M., Pabalan, R. T.: Review of Empirical Thermodynamics Data for Uranyl Silicate Minerals and Experimental Plan. Center for Nuclear Waste Regulatory Analyses, San Antonio, Texas, CNWRA 95-014, 43 p. (1995).
11. Cesbron, F., Ildefonse, I., Sichere, M.: New Mineralogical Data on Uranophane and Beta-uranophane; Synthesis of Uranophane. Mineralogical Magazine 57, 301-308 (1993).

12. ICDD: Powder Diffraction File PDF-2 Database Sets 1-43. International Centre for Diffraction Data, Swarthmore, PA (1993).

13. ICDD: Mineral Powder Diffraction File Data Book. International Centre for Diffraction Data, Swarthmore, PA (1986).

14. Nguyen, S. N., Silva, R. J., Weed, H. C., Andrews, J. E.: Standard Gibbs Free Energy of Formation at the Temperature of 303.15 K of Four Uranyl Silicates: Soddyite, Uranophane, Sodium Boltwoodite, and Sodium Weeksite. Journal of Chemical Thermodynamics 24, 359-376 (1992).

15. Chen, F., Ewing, R. C., Clark, S. B.: The Gibbs Free Energies and Enthalpies of Formation of U^{6+} Phases: An Empirical Method of Prediction. American Mineralogist 84, 650-664 (1999).

16. Wolery, T.: EQ3/6, A Software Package for Geochemical Modeling of Aqueous Systems. UCRL-MA-110662 PT1, Lawrence Livermore National Laboratory, Livermore, CA (1992).

17. Grenthe, I., Fuger, J., Konings, R. J. M., Lemire, R. J., Muller, A. B., Nguyen-Trung, C., Wanner, H.: Chemical Thermodynamics of Uranium, Chemical Thermodynamics Series Vol. 1, Nuclear Energy Agency (NEA), Elsevier, New York (1992).

18. Perez, I., Casas, I., Martin, M., Bruno, J.: The Thermodynamics and Kinetics of Uranophane Dissolution in Bicarbonate Test Solutions. Geochimica et Cosmochimica Acta 64, 4, 603-608 (2000).

19. Finch, R. J., Ewing, R. C.: Alternation of Natural UO_2 under Oxidizing Conditions from Shinkolobwe, Katanga, Zaire: A Natural Analogue for the Corrosion of Spent Fuel. Radiochimica Acta 52/53, 395-401 (1991).

Table 1. Starting U concentrations and pH of uranophane solubility experiment test solutions.

Test Label	U ($mol \cdot L^{-1}$)	pH
A	1.0×10^{-5}	6.1
B	3.2×10^{-6}	6.05
C	1.1×10^{-6}	6.07
D	3.2×10^{-7}	6.14
E	1.0×10^{-7}	6.18

9/12

Table 2. Solution pH, logarithms of activities of Ca^{2+}, $SiO_2(aq)$, and UO_2^{2+}, and calculated logarithm of reaction quotients (log Q) for uranophane in test solutions at the 5, 6, and 7 week sampling intervals.

Test Label	Sampling time (wks)	pH	log[Ca^{2+}]	log[$SiO_2(aq)$]	log[UO_2^{2+}]	log Q
A	5	5.47	-2.25	-2.91	-6.51	11.71
	6	5.46	-2.25	-2.90	-6.72	11.28
	7	5.44	-2.24	-2.89	-6.64	11.34
B	5	5.57	-2.25	-2.90	-6.81	11.74
	6	5.55	-2.25	-2.90	-7.19	10.89
	7	5.65	-2.24	-2.88	-7.04	11.83
C	5	6.57	-2.23	-2.88	-8.83	13.77
	6	6.71	-2.22	-2.87	-8.84	14.62
	7	6.68	-2.21	-2.84	-8.91	14.36
D	5	6.65	-2.24	-2.89	-9.06	13.76
	6	6.80	-2.23	-2.87	-9.49	13.84
	7	6.75	-2.23	-2.87	-9.39	13.76
E	5	6.58	-2.23	-2.88	-8.73	14.02
	6	6.70	-2.22	-2.87	-8.94	14.33
	7	6.70	-2.22	-2.86	-8.85	14.55

Figure Captions

Fig. 1. X-ray diffraction pattern of synthesized uranophane compared to a reference pattern taken from the International Centre for Diffraction Data database [12]. The synthetic uranophane XRD pattern was obtained using an automated (RADIX) Siemens D-500 x-ray diffractometer (CuKα radiation, Ni filter, 40 kV, 37 mA; scan 2°-70° 2θ at 0.02° step; count time of 1.0 s). The inset image is a scanning electron photomicrograph of the synthesized uranophane.

Fig. 2. The pH (a) and concentrations of Ca (b), Si (c), and U (d) in the uranophane solubility tests plotted as a function of time. The starting U concentration for Test A (1e-5 mol · L^{-1}) at time 0 (d) is not shown.

Fig. 3. Net moles of Ca (a), Si (b), and U (c) released to solution as a function of time in the uranophane solubility tests.

Fig. 4. Relative number of moles of Ca and Si released in the uranophane solubility tests. Dashed lines have slopes of 0.5 and 2.0 and are included for illustrative purposes (see text for explanation). Solid line with arrow shows trend in solution sampling time.

Fig. 5. Logarithmic activity diagram of $UO_2^{2+}/(H^+)^2$ versus $SiO_2(aq)$ illustrating position of uranophane solubility test solution chemistries in the last 4 sampling intervals with respect to the solubility limit of soddyite and schoepite. The solubility limit for soddyite is based on data from Chen et al. [15]. A single solution chemistry taken from a soddyite dissolution experiment conducted by Nguyen et al. [14] is also plotted. The solubility limit for schoepite is based on data from Grenthe et al. for $UO_2 \cdot 2H_2O(s)$ [17].

Fig. 6. Logarithmic activity diagram of $UO_2^{2+}/(H^+)^2$ versus $SiO_2(aq)$ versus $Ca^{2+}/(H^+)^2$ illustrating the position of E-type (tests C, D, and E) solution chemistries for the last 4 sampling intervals with respect to the solubility limit of uranophane calculated with data from Chen et al. [15]. With respect to the theoretical uranophane solubility limit from Chen et al. [15] shown in the diagram, solution chemistries plotting above the plane of the solubility limit are supersaturated with uranophane and those plotting below the plane are undersaturated with uranophane. However, mass transfer analyses in this study indicate that all plotted solutions were undersaturated with respect to uranophane.

Fig. 1

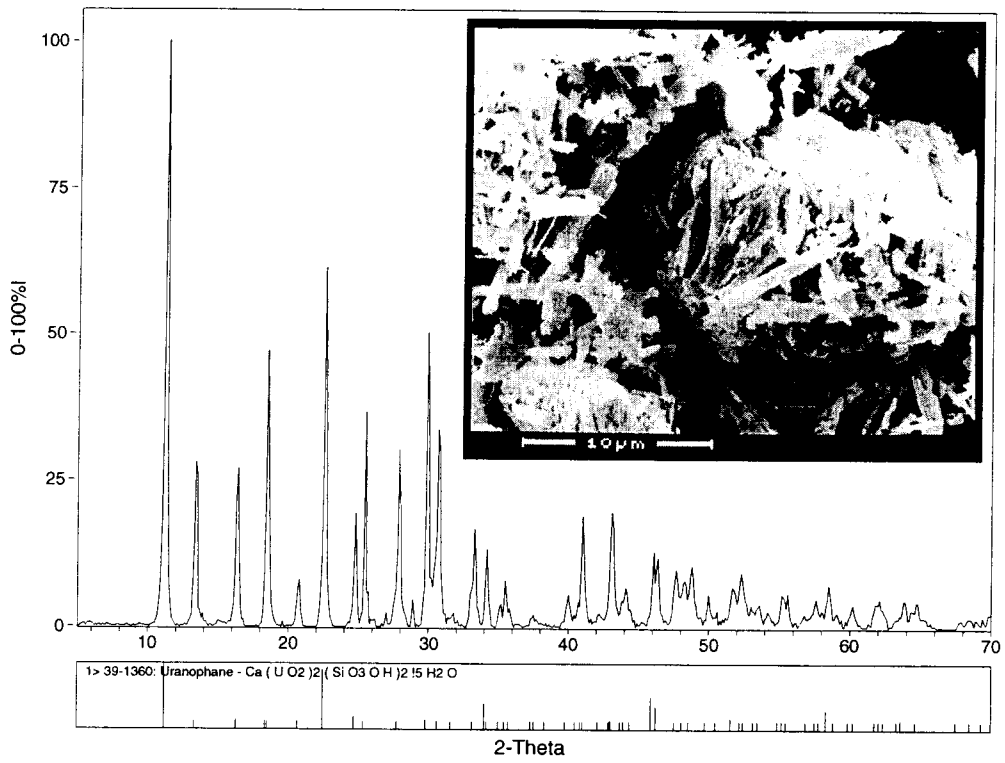
100
75
50
25
0
0-100%I
10
20
30
40
50
60
70
10 µm
1> 39-1360: Uranophane - Ca (U O2)2(Si O3 O H)2 !5 H2 O
2-Theta

Fig. 2

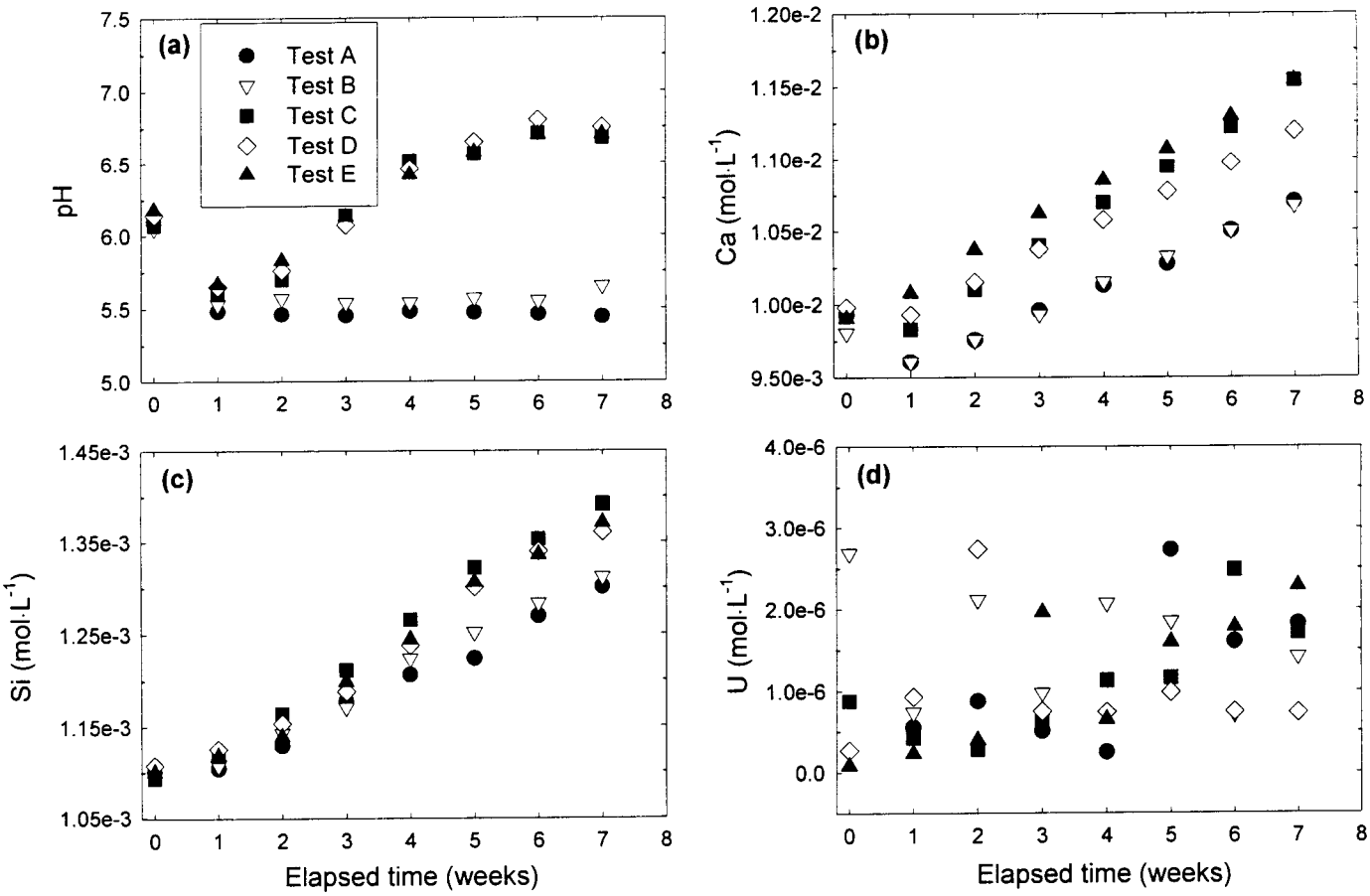
(a)
Test A
Test B
Test C
Test D
Test E
pH
(b)
Ca (mol·L-1)
(c)
Si (mol·L-1)
(d)
U (mol·L-1)
Elapsed time (weeks)
Elapsed time (weeks)

Fig. 3

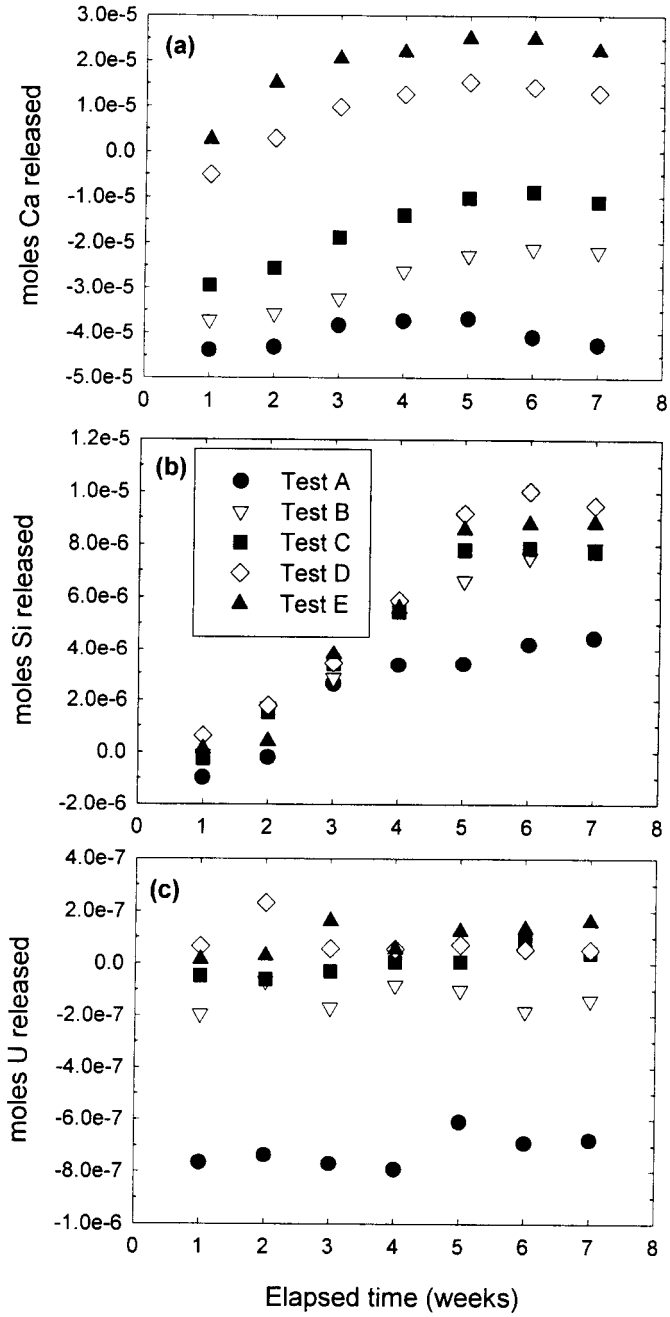
(a)
moles Ca released
3.0e-5
2.0e-5
1.0e-5
0.0
-1.0e-5
-2.0e-5
-3.0e-5
-4.0e-5
-5.0e-5
(b)
moles Si released
1.2e-5
1.0e-5
8.0e-6
6.0e-6
4.0e-6
2.0e-6
0.0
-2.0e-6
Test A
Test B
Test C
Test D
Test E
(c)
moles U released
4.0e-7
2.0e-7
0.0
-2.0e-7
-4.0e-7
-6.0e-7
-8.0e-7
-1.0e-6
0 1 2 3 4 5 6 7 8
Elapsed time (weeks)

Fig. 4

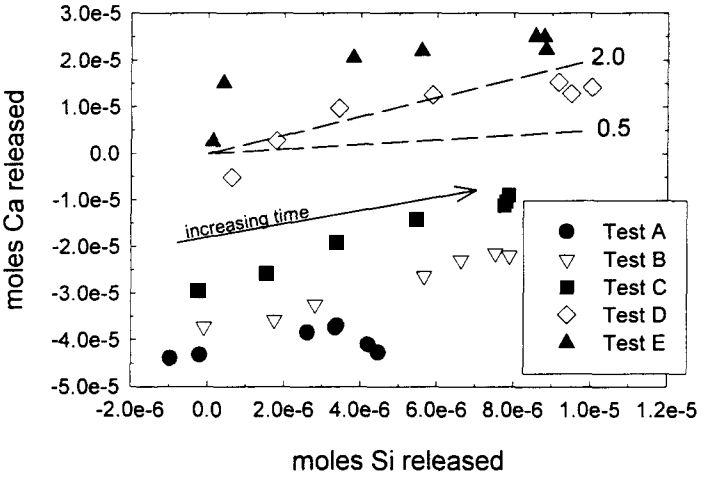
3.0e-5
2.0e-5
1.0e-5
0.0
-1.0e-5
-2.0e-5
-3.0e-5
-4.0e-5
-5.0e-5
-2.0e-6
0.0
2.0e-6
4.0e-6
6.0e-6
8.0e-6
1.0e-5
1.2e-5
moles Ca released
moles Si released
2.0
0.5
increasing time
Test A
Test B
Test C
Test D
Test E

Fig. 5

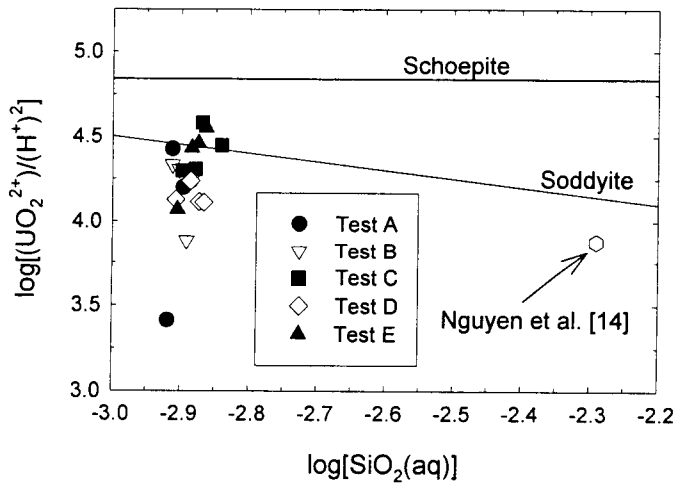
Schoepite
Soddyite
Test A
Test B
Test C
Test D
Test E
Nguyen et al. [14]
5.0
4.5
4.0
3.5
3.0
-3.0
-2.9
-2.8
-2.7
-2.6
-2.5
-2.4
-2.3
-2.2
log[(UO2 2+)/(H+)2]
log[SiO2(aq)]

Fig. 6

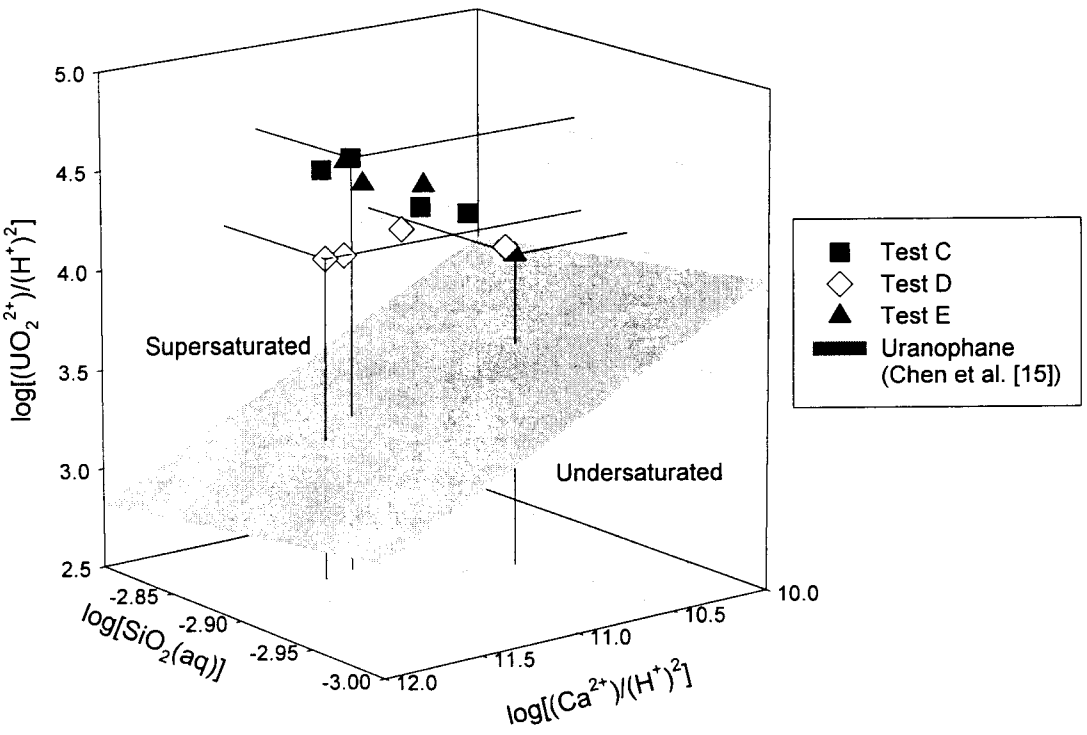
5.0
4.5
4.0
3.5
3.0
2.5
log[(UO2 2+)/(H+)2]
Supersaturated
Undersaturated
-2.85
-2.90
-2.95
-3.00
log[SiO2(aq)]
12.0
11.5
11.0
10.5
10.0
log[(Ca2+)/(H+)2]
Test C
Test D
Test E
Uranophane
(Chen et al. [15])